

Article

# Dual-Polarized Reconfigurable Manipulation Based on Flexible-Printed Intelligent Reflection Surface

Xiaozhe Jia , Hongrui Tan, Xinyu Dong, Fujun Ye, Haoyang Cui and Lei Chen \* 

College of Electronics and Information Engineering, Shanghai University of Electric Power, Shanghai 200090, China

\* Correspondence: leichen\_suep@163.com

**Abstract:** In the background of 6G communication requiring a high data rate and energy efficiency, global coverage and connectivity, as well as high reliability and low latency, most existing reconfigurable metasurfaces face limitations in flexibility, integrability, energy consumption, and cost. This paper proposes a dual-polarized intelligent reflection surface (IRS) based on a paper-based flexible substrate as a solution. The proposed design uniquely enables the independent control of two orthogonally polarized electromagnetic waves to achieve customized scattering effects. Compared to conventional reconfigurable intelligent surfaces using PCB technology and active components, this design utilizes paper as the substrate material combined with conductive ink and silver ink, significantly reducing production costs and process complexity. The manufacturing cost is only about one-tenth of the traditional PCB solutions. This approach is not only cost-effective but also excels in both flexibility and portability. These attributes signify its suitability for a broader range of potential applications, encompassing areas where traditional RIS may be impractical due to cost, rigidity, or complexity constraints. By drawing rotationally symmetric small metal block structures on paper using silver ink, four structures are designed that achieve a phase difference of 90 degrees for both x-polarized and y-polarized wave incidences at the resonant frequency of 4.5754 GHz, realizing independent phase modulation. The dual-polarized flexible 2-bit intelligent reflection surface consists of  $20 \times 20$  unit cells, and six different coding patterns are designed for single-beam and dual-beam design based on different scattering angles. The experimental results show that this polarization-independent flexible 2-bit intelligent reflection surface structure successfully allows independent control of two orthogonally polarized electromagnetic waves, enabling customized scattering effects. The experimental results are highly consistent with the simulation results. The independent control of two orthogonal polarized electromagnetic waves is a key feature of our design, enabling more flexible and effective signal coverage in complex urban environments. This precise control over polarization not only enhances the adaptability of the system but also offers practical solutions for real-world applications, particularly in meeting the growing demands of urban communication. The proposed metasurface based on paper-based flexible substrate is low-cost and highly portable, and the polarization independence provides more degrees of freedom for the metasurface, which is beneficial for more precise and efficient beam control and can be applied in the field of communication, especially 6G communication and IRS wireless communication. In addition, it also has broad application prospects in radar systems and remote sensing applications.



**Citation:** Jia, X.; Tan, H.; Dong, X.; Ye, F.; Cui, H.; Chen, L. Dual-Polarized Reconfigurable Manipulation Based on Flexible-Printed Intelligent Reflection Surface. *Photonics* **2024**, *11*, 69. <https://doi.org/10.3390/photonics11010069>

Received: 6 November 2023

Revised: 25 December 2023

Accepted: 29 December 2023

Published: 8 January 2024



**Copyright:** © 2024 by the authors. Licensee MDPI, Basel, Switzerland. This article is an open access article distributed under the terms and conditions of the Creative Commons Attribution (CC BY) license (<https://creativecommons.org/licenses/by/4.0/>).

**Keywords:** intelligent reflection surface; dual-polarized reconfigurable metasurface; low-cost manufacturing; flexible-printed

## 1. Introduction

Although the fifth generation (5G) wireless network is still in the deployment phase worldwide, both the academic and industrial sectors have already cast their eyes on envisioning the sixth generation (6G) wireless network. The deployment of 6G requires

meeting a series of stringent requirements, such as ultra-high data rates and energy efficiency, global coverage and connectivity, as well as high reliability and low latency [1,2]. To achieve these goals, the development of new and innovative technologies has become urgent. In this context, metasurfaces have garnered widespread attention as a potential technological solution. Metamaterials are artificially engineered electromagnetic structures composed of subwavelength unit cells arranged periodically or non-periodically, capable of controlling electromagnetic waves [3] by designing the unit cell structure and their arrangement [4–6]. Metasurfaces are the two-dimensional equivalent of metamaterials, possessing a low profile, easier fabrication, and the same remarkable ability to manipulate electromagnetic waves [7–13]. They can precisely control the amplitude, phase, and polarization of incident electromagnetic waves, demonstrating tremendous potential in improving the performance and functionality [14–16] of communication systems [17–19]. In order to utilize advanced information processing technology to achieve highly controlled and efficient manipulation of electromagnetic information, as well as to improve the efficiency and accuracy of information transmission and processing, it is necessary to establish a connection between metasurfaces and digital information. In 2014, the Cui Tie Jun team proposed the concept of coding metasurfaces [20,21], incorporating digital binary coding into the design of metasurfaces and enabling free control of electromagnetic waves by setting coding sequences. The emergence of coding metasurfaces, as well as the introduction of the generalized Snell's law, has created conditions for the development of reconfigurable metasurfaces [22,23], also known as intelligent reflection surfaces (IRS). These reconfigurable metasurfaces can be controlled to manipulate electromagnetic waves in real time, providing adaptive and programmable functionalities. Existing reconfigurable metasurfaces are typically made with printed circuit board (PCB) technology, utilizing rigid substrates such as glass fiber-reinforced epoxy resin (FR4) and metallic structures as the top layer. This not only leads to extended production cycles but also restricts these solutions' applicability in scenarios requiring rapid deployment or flexibility. Additionally, most reconfigurable metasurfaces rely on active components, like PIN diodes or varactor diodes [24,25]. Designs incorporating active devices encounter limitations in large-scale communication systems due to their high energy consumption. Therefore, while these metasurfaces have demonstrated impressive functionalities [26–31], they face limitations in terms of flexibility, integrability, power consumption, and cost in the context of 6G communications. Especially for most communication scenarios, the cost and power consumption are key indicators of applications. Also, the polarization insensitivity will be more suitable for most mobile communication applications. Potential future directions for this technology encompass the integration of dual-polarized IRS with advanced communication systems for a broader range of applications, including smart transportation and urban security; the exploration of its feasibility in large-scale network deployment within 6G networks; and the advancement of its adaptability to diverse environmental conditions and intelligent control for efficient signal management. Further research in these areas is expected to open up new possibilities for its practical application.

In this paper, we propose a solution based on conductive ink metal structures and paper as a flexible substrate, creating a polarization-insensitive intelligent reflection surface with 2 bits. Compared to traditional reconfigurable metasurfaces, our dual-polarized flexible 2-bit intelligent reflection metasurface design utilizes paper-based materials, circumventing the need for PCB technology. It offers a more energy-efficient and convenient manufacturing alternative, suitable for a wide range of applications where traditional methods are inadequate. Specifically, conductive ink is used to draw the basic metal structures on the top layer, while silver-ink is employed to connect these basic metal structures for achieving the phase response of the dual-polarized metasurface. The presence or absence of silver-ink plotted metal blocks in the x and y directions is used to design four structures that satisfy both a 90-degree phase difference in the reflection phase and independent phase control on two orthogonal polarizations. By mapping the reflected phase states of these four structures to a binary code from 0 to 3, this is used to design the order of

arrangement on the metasurface. This allows for specific phase and amplitude distributions and, furthermore, different beam deflections. Experimental results show that this flexible dual-polarized 2-bit smart reflection surface structure successfully achieves independently controlled reflection phases of two orthogonally polarized electromagnetic waves. The incorporation of 2-bit phase modulation provides more degrees of freedom for controlling electromagnetic waves, contributing to more precise and efficient beam control. Moreover, the portability and low-cost characteristics of paper-based metasurfaces make them highly promising for wireless communication applications utilizing IRS. In the introduction, this paper discusses the requirements and technological challenges of 6G communications, highlighting the limitations in flexibility, integrability, energy consumption, and cost faced by current research on reconfigurable metasurfaces. Subsequently, in Section 2, we analyze the principles and advantages of the proposed paper-based flexible substrate intelligent reflection surface (IRS) as a solution, along with the design methods for these metasurface units. Following this, in Section 3, we present the far-field outcomes for six different coding modes, achieving distinct dual-beam and single-beam patterns. In Section 4, we describe the setup of our test environment and its significance, as well as how to effectively conduct experimental designs. Section 5 then delves into the experimental findings, confirming their high consistency with the simulation results and discussing the reasons for any discrepancies. Finally, in the conclusion, we summarize the research outcomes and analyze the prospective applications and future outlook for this technology in various domains.

## 2. Principle and Design

Reconfigurable metasurfaces typically consist of numerous units, each containing tiny structures for manipulating electromagnetic waves. When electromagnetic waves incident on the metasurface, these microstructures induce reflection and scattering of the incident waves. Specific phase and amplitude distributions on the metasurface can be realized by coding cells with different phase and amplitude states and designing coding sequences. This allows precise control of the amplitude, phase, and direction of the reflected wave. Furthermore, once the phase and amplitude distribution of the reconfigurable metasurface are determined, manipulation of the scattered field can be achieved via the far-field scattering function formula:

$$f_e(\theta, \varphi) = \sum_{m=1}^N \sum_{n=1}^N A_{mn} \exp\{-i\{\varphi(m, n) + kD \sin\theta[(m - 0.5)\cos\varphi + (n - 0.5)\sin\varphi]\}\}, \quad (1)$$

where  $\theta$  and  $\varphi$  represent the elevation and azimuth in any direction. In addition,  $A_{mn}$  and  $\varphi(m, n)$  signify the amplitude and phase responses of the metasurface element ( $m$  row and  $n$  column), respectively, while  $f_e(\theta, \varphi)$  elucidates the lattice's mode function. A more detailed derivation of this formula can be found in [32]. Based on this formula, we can control the scattering direction and quantity of light beams by designing unique phase and amplitude distributions. In this paper, we introduce a dual-polarized flexible 2-bit intelligent reflection surface. Unlike traditional reconfigurable metasurfaces that rely on active components and are manufactured using PCB technology, our novel IRS design employs paper-based materials and eliminates the need for active elements. This innovation simplifies the manufacturing process, reduces costs, and lowers energy consumption. Due to its flexibility and lightweight nature, this new type of IRS can be applied in a broader range of scenarios, such as wearable devices and temporary communication systems. Moreover, its dual-polarization and 2-bit coding capabilities offer enhanced flexibility and efficiency in controlling electromagnetic waves, making it particularly suitable for the demands of 6G communication technologies. Overall, our design represents not only a technical innovation but also paves a new direction for the advancement of future communication technologies. As shown in Figure 1, fabricated by drawing the top-layer basic structure on paper using conductive ink and connecting the basic structure with small metal blocks composed of silver ink. An air layer and a bottom metal layer with a conductivity of  $5 \times 10^7$  S/m are employed to support the paper. The desired phase and amplitude distribution of the metasurface is realized by designing different distributions of small metal blocks. The designed

IRS can control the scattering direction of the beam and produce single or multiple beams. These units have a rotationally symmetric metric structure, and the metasurface comprising these units is capable of controlling electromagnetic waves independently under two orthogonal polarizations. This provides greater degrees of freedom than conventional single-polarization control methods.

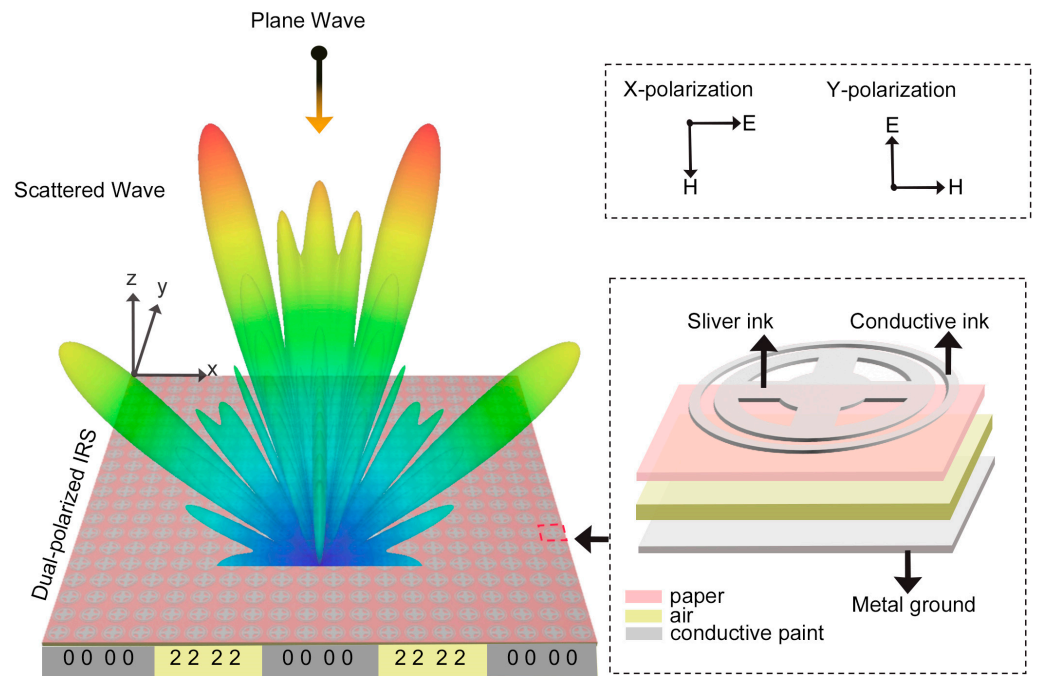


**Figure 1.** The schematic of the dual-polarized 2-bit intelligent reflection surface. By adjusting the distribution of small metal elements composed of silver ink, specific phase, and amplitude distributions can be achieved, enabling control over the beam scattering direction and quantity. Moreover, the rotationally symmetric structure allows the IRS to independently manipulate electromagnetic waves in two orthogonal polarization states.

The structure and dimensional parameters of the unit of the dual-polarized intelligent reflection surface are shown in Figure 2a–c. The element of the metasurface consists of four layers of materials, with the top layer being a metallic layer composed of conductive ink and silver ink, with a conductivity of  $5 \times 10^7$  S/m and a thickness of 0.02 mm. The outer radius of the large annulus is  $r_2 = 12.8$  mm, the outer radius of the small annulus is  $r_1 = 10.5$  mm, and the radius of the center circle is  $r = 4.5$  mm. The eight metal blocks connecting these three parts have a width of  $d = 4$  mm. The length of the four metal blocks connecting the center circle and the small annulus is  $m = 4.23$  mm, while the length of the four metal blocks connecting the small annulus and the large annulus is  $n = 1.32$  mm. The intermediate two layers consist of a paper layer and an air layer, which are, respectively, marked with pink and yellow in Figure 2a–c. The dielectric constant of the paper layer is  $\epsilon_1 = 2.5$ , with a thickness of  $h_1 = 0.1$  mm, while the dielectric constant of the air layer  $\epsilon_2 = 1$ , with a thickness of  $h = 5$  mm. The bottom layer is a fully covered metal layer with a thickness of 0.018 mm and a conductivity of  $5 \times 10^7$  S/m. The period of the unit is  $a = 30$  mm. Other variable dimensions marked in the figures:  $w_1 = 1$  mm,  $w_2 = 2$  mm. Due to the complex interactions among unit structures, analytical calculations only offer a coarse understanding of their effect on electromagnetic waves. Thus, we obtain parameter values via a simulation-based optimization process. The electrical length along the polarization direction determines the unit’s resonant characteristics, which in turn influence phase changes. In simulations, we prioritize key geometric dimensions affecting electrical length along the polarization direction, and then fine-tune other dimensions for an optimized design. For instance, when the unit’s top metallic structure is distributed as in Figure 2b and is x-polarized, critical

geometric parameters include  $m$ ,  $w_1$ ,  $w_2$ ,  $n$ , and  $r$  in the  $x$ -direction. Notably, our proposed unit structure is rotationally symmetric. After optimizing these parameters, we further refine the  $y$ -dimension, such as the  $d$  parameter. The inner circle, inner ring, and outer ring are connected by 8 metal blocks and labeled in Figure 2a. To achieve polarization independence, the top-layer metal structure is designed to be rotationally symmetric. The unit is simulated using the CST Microwave Studio electromagnetic simulation software based on the finite element method. The port conditions are set as Floquet, and the  $z$ -axis and  $y$ -axis directions use unit cell periodic boundary conditions. The reflected phase and amplitude responses of the unit cell under  $x$ -polarized and  $y$ -polarized incidence are consistent, and the phase and amplitude response curves of the unit under  $y$ -polarized incidence are shown in Figure 2d,e, respectively. The four curves in the figure represent four different cases when the top-layer metal structure is rotationally symmetric, and the grey marks indicate the position of the resonant frequency. At the resonant frequency of 4.5754 GHz, the phase differences in the four states are  $29.9^\circ$ ,  $-58.9^\circ$ ,  $117.1^\circ$ , and  $-149.5^\circ$ , satisfying a 90-degree phase difference. The change in phase is related to the electrical length, and modifying the size and arrangement of the metallic blocks effectively alters this electrical length, thereby shifting the phase of the reflected wave. The four states of the unit cell, state0-state3, are shown in Figure 2f, where small metal blocks 5–7 do not exist, all eight small metal blocks do not exist, all eight small metal blocks exist, and small metal blocks 1–4 do not exist, respectively. At the same time, these four states are encoded as 0–3. Additionally, the four states of the unit exhibit a high amplitude response greater than  $-0.8$  dB, indicating high reflection efficiency when manipulating the reflected EM waves. The energy efficiency is at least about 83% according to the reflected amplitude.

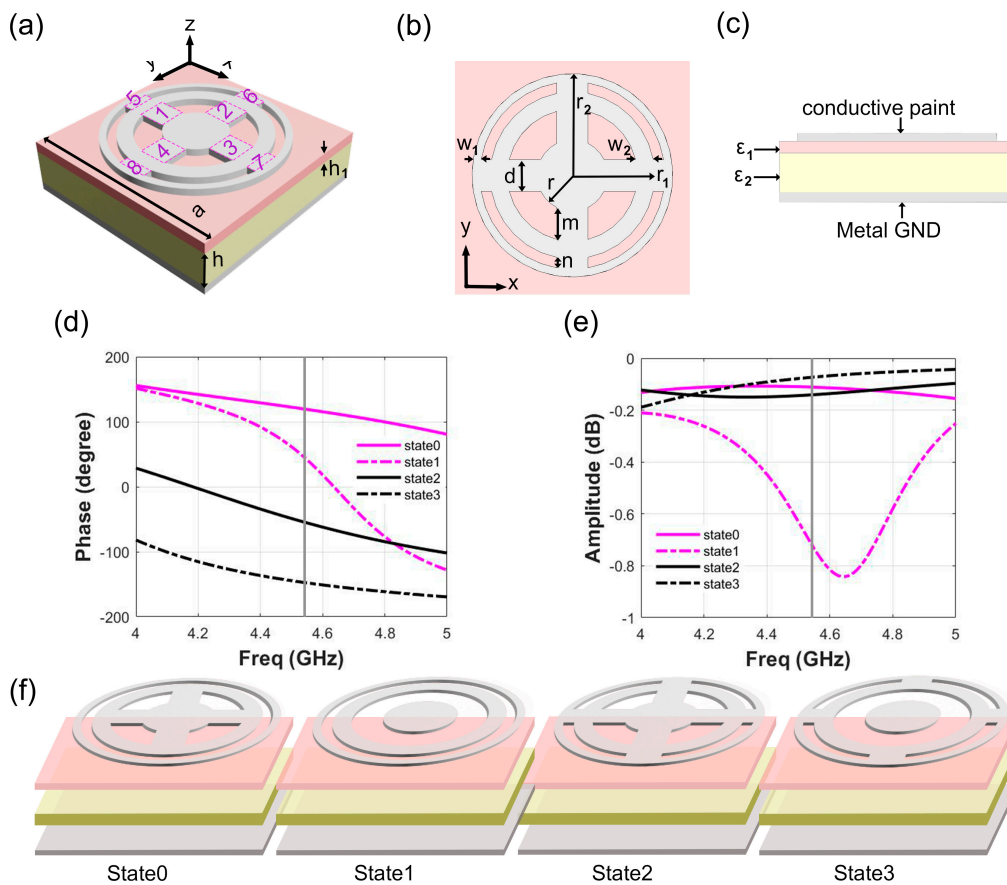


**Figure 2.** Illustration of the unit of dual-polarized metasurface for wavefront manipulation and electromagnetic response: (a) 3D perspective view of the unit; (b) front view of the unit; (c) side view of the unit; (d,e) reflect the phase response and amplitude response curves of the unit under

y-polarized incidence at the resonant frequency of 4.5754 GHz, respectively; (f) structural diagram of the four states with a 90-degree phase difference.

### 3. Simulation Results

We designed six different coding sequences and simulated the beam-steering capability of the dual-polarized 2-bit metasurface under plane-wave excitation in an open boundary setting in CST software, simulating the environment of a standard microwave chamber. The experimental sample consists of  $20 \times 20$  unit cells, with an overall size of  $600 \times 600 \text{ mm}^2$ . Since the bottom layer of the sample is a metal layer that does not allow the electromagnetic waves to pass through, only the reflection behavior of the dual-polarized 2-bit metasurface needs to be considered. Figure 3 presents the 3D far-field results of the metasurface scattering field simulation for six different coding sequences under x-polarized and y-polarized conditions at the resonant frequency of 4.5754 GHz. In Figure 3a–f, the left panel displays the patterns, while the middle panel and right panel display the simulation results under y polarization and x polarization conditions, respectively. Figure 3a–f include the simulation verification of periodic coding sequences for single-beam and dual-beam scattering effects, with coding sequences as follows: “00112233001122330011”, “00011122233300011122”, “00001111222233330000”, “00002222000022220000”, “00000022222200000022”, and “00000000222222220000”. From Figure 3, it can be observed that at the resonant frequency of 4.5754 GHz, the simulation results of the metasurface patterns in Figure 3a–f are almost identical under x-polarized and y-polarized conditions, with consistent beam-deflection angles and similar energy. This indicates that the designed 2-bit coding metasurface meets the dual-polarized requirements. Furthermore, it can be seen from Figure 3a–c that single-beam scattering is generated, with most of the energy concentrated on the main beam. Meanwhile, the deflection angle decreases with the increase in the coding sequence period, with the beam deflection angles for Pattern A to Pattern C ranging from  $15^\circ$  to  $9^\circ$  and finally to  $7^\circ$ . On the other hand, Figure 3d–f show clear dual-beam scattering, similar to the conclusions obtained from Figure 3a–c, with most of the energy concentrated on the two main beams and a very low energy of the sidelobe beams. The deflection angle of the dual beam decreases with the increase in the coding sequence period, from  $\pm 14^\circ$  for Pattern D to  $\pm 9^\circ$  for Pattern E and finally to  $\pm 7^\circ$  for Pattern F. Overall, the simulation results show that the proposed IRS has the ability to independently control electromagnetic waves under two orthogonal polarizations. By designing specific phase and amplitude distributions, the metasurface can control the scattering direction and the number of beams, and different deflection angles can be obtained by changing the periodic coding sequence, thus achieving customized scattering effects.

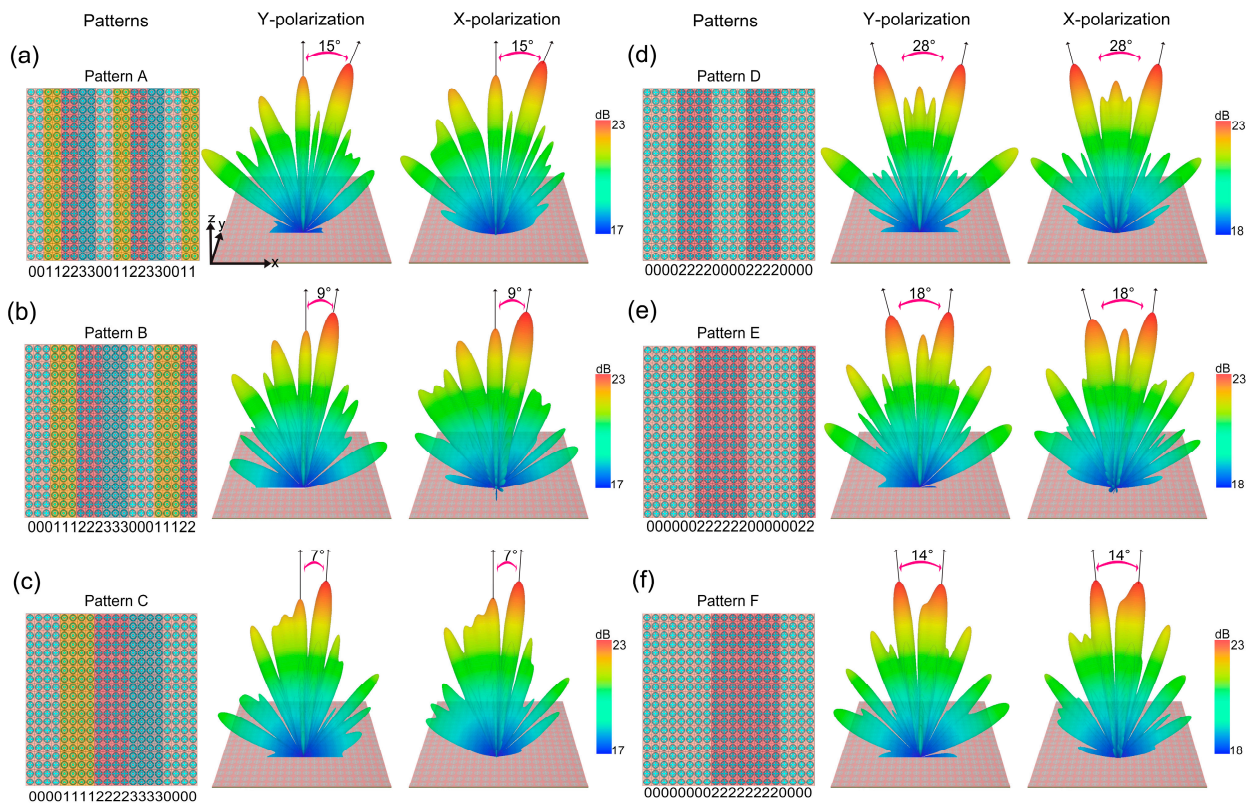


**Figure 3.** Designed six patterns of single-beam and dual-beam patterns of the metasurface and 3D far-field simulation results under two orthogonal polarizations at the resonant frequency of 4.5754 GHz: (a) Pattern A with the coding sequence “00112233001122330011”; (b) Pattern B with the coding sequence “00011122233300011122”; (c) Pattern C with the coding sequence “00001111222233330000”; (d) Pattern D is represented by the coding sequence “00002222000022220000”; (e) Pattern E is represented by the coding sequence “00000022222200000022”; (f) Pattern F is represented by the coding sequence “00000000222222220000”.

#### 4. Experimental Configuration

In order to ensure that there are no additional refractions or reflections of electromagnetic waves during the experimental process to affect the measurement results, the far-field test of the proposed paper-based dual-polarized IRS is conducted in a standard microwave chamber. The specific parameters of the receiver and transmitter are shown in Table 1. As shown in Figure 4a, the metasurface sample and the feed horn antenna are fixed on a mechanical turntable. A small broadband rectangular horn antenna is used as the linearly polarized feed source, placed 1.5 m away from the metasurface sample to simulate the excitation of approximately plane waves. The receiving horn antenna is a large aperture broadband horn antenna placed approximately 10 m away from the turntable. Figure 4b shows IRS samples with sequences of “00002222000022220000” and “00112233001122330011”, composed of  $20 \times 20$  unit cells. First, the outline of the top-layer metal structure, including the basic structure and eight small metal block structures, is printed on A4 paper. Then, the area of the basic structure outline on the A4 paper is coated with conductive ink, and the small metal block structures made of silver ink are arranged according to the designed sequence to form the top-layer metal layer. In our design, both types of inks mainly used conductive properties, allowing for the modification of the unit’s electrical characteristics by drawing or printing the unit’s structure, thereby influencing the electromagnetic response and causing phase changes. Specifically, in our experiment, conductive ink provides basic conductivity, used for printing fundamental metal structures like rings. The printability of this ink makes it highly suitable for use on flexible substrates, forming the necessary conductive structures and facilitating initial

electromagnetic characteristic adjustments. On the other hand, silver ink is primarily used for manually fine-tuning the metal structures, offering a one-time modification opportunity. Silver-ink connects these metal blocks to achieve the phase response of a dual-polarized metasurface. We chose not to print directly with silver ink due to its tendency to clog the printing equipment during the process. It is worth noting that in practical measurements, conductive patterns can be reconstructed not only using silver ink but also via direct printing. The A4 paper is supported by a stack of foam that is 5 mm thick. Since the dielectric constant of the foam is 1.04, which closely approximates the dielectric constant of air, the effect of replacing the air layer with the foam layer has a negligible impact on the scattering characteristics of the metasurface. During the experiment, the turntable rotates the sample in a two-dimensional plane, allowing the receiving horn antenna to receive scattered signals from different directions. By analyzing the intensity and phase information of these signals, we can obtain the scattering characteristics of the proposed IRS in different directions.

**Table 1.** Table of relevant parameters of feed antenna and receive antenna in experimental configuration.

Antenna	Frequency Range	Gain	Polarization	Aperture Size
Transmitter	2 GHz–18 GHz	6 dBi	Linear	80 mm
Receiver	2 GHz–18 GHz	18 dBi	Linear	250 mm

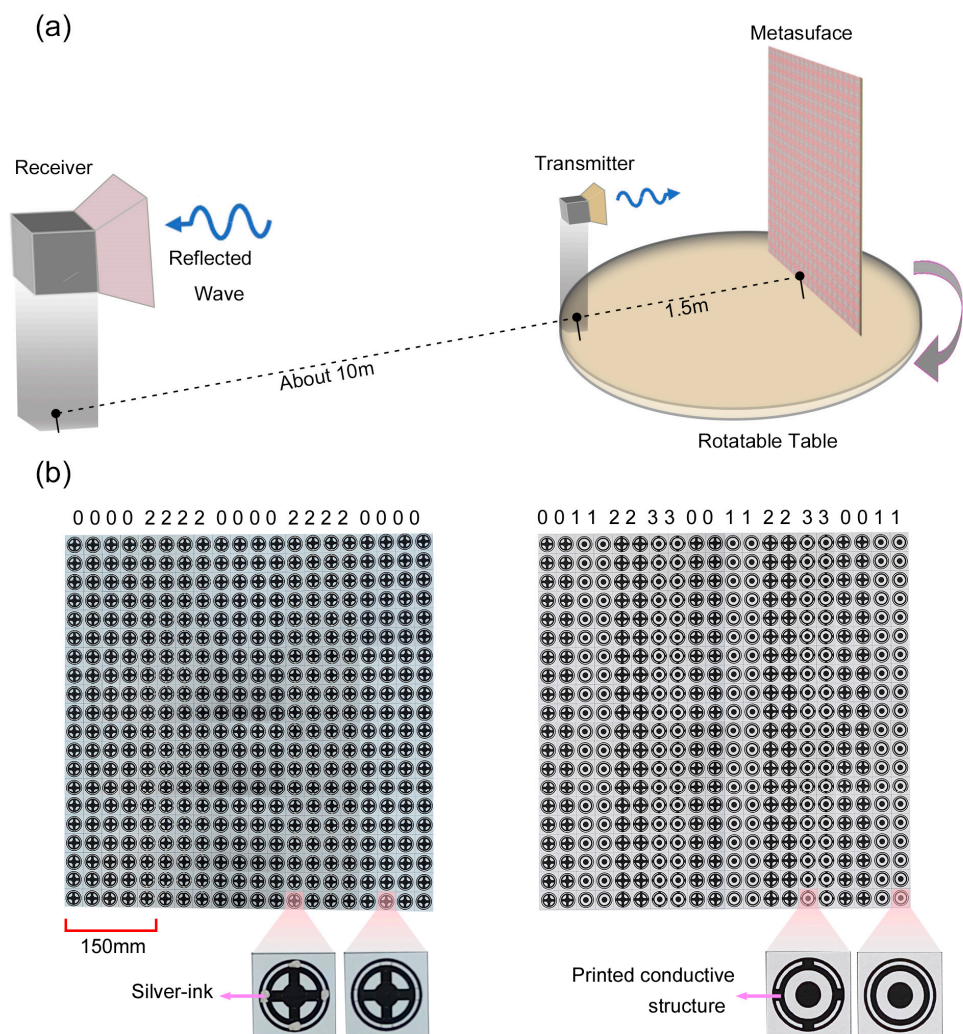


**Figure 4.** Schematic diagram of the IRS sample and the measured configuration: (a) configuration of experimental environment for far-field testing; (b) details of the fabricated IRS samples with sequences “00002222000022220000” and “00112233001122330011”.

### 5. Results Discussion

In Figure 5, we compare the far-field measurement results with the simulation results for different patterns at 4.5754 GHz, represented by the red and blue lines, respectively. Figure 5a–c, respectively, represent the single-beam results for pattern A to pattern C, with beam deflection angles of 15°, 10°, and 7°, respectively. Figure 5d–f represent the dual-beam results for pattern D to pattern F, with beam deflection angles of ±14°, ±9°, and ±7°, respectively. From Figure 5a–f, it can be seen that the red and blue lines are highly overlapped in the −30° to +30° range. In addition, high consistency is also maintained in other regions, indicating a good agreement between the measurement results and the simulation results. The deviation of the beam deflection angle between the experimental and simulation results is within ±1%, and the amplitude error between the measurement and simulation results is within ±0.3 dB. The measured efficiency is about 66%, according to the experimental results. There are small errors between the measurement and simulation results, which may be caused by several factors: (1) Manual operation during the entire experiment may introduce errors; (2) errors caused by the non-ideal excitation of the horn antenna; and (3) substituting the air layer with a foam layer, even though the dielectric constant of foam closely approximates the dielectric coefficient of air, this minute division might manifest in the practical measurements and culminate in inaccuracies.

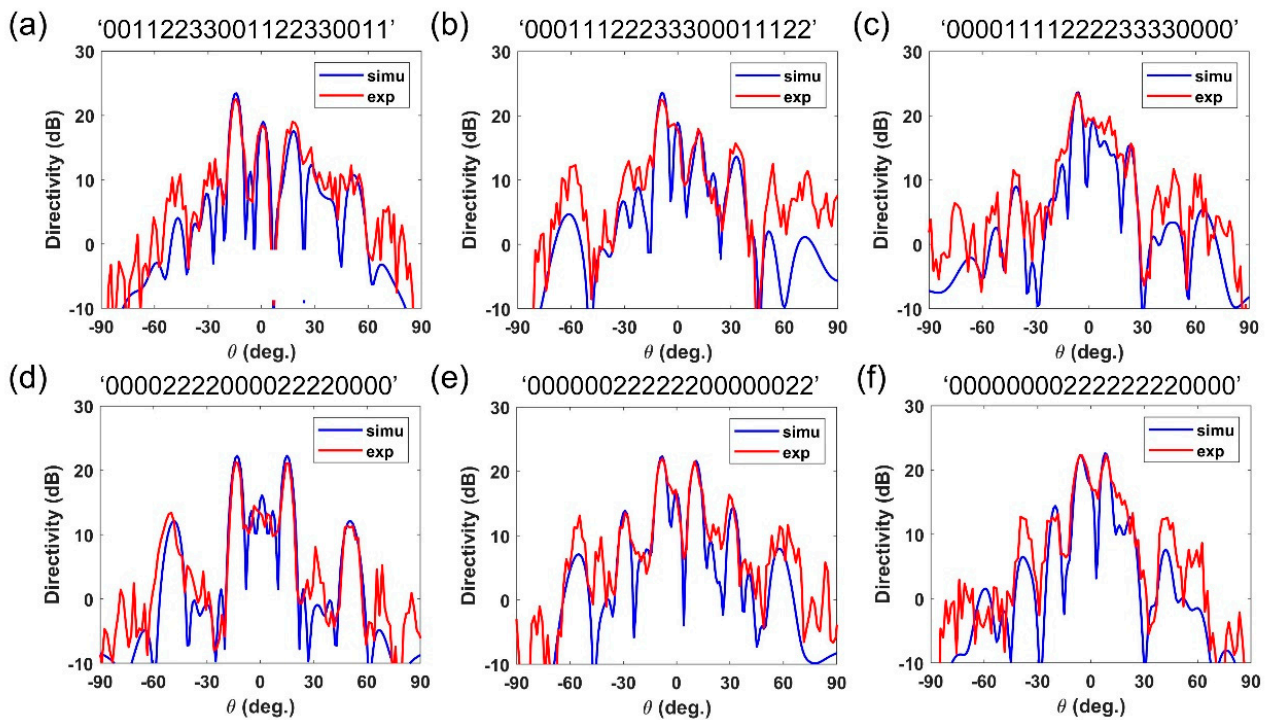


**Figure 5.** Far-field measurement results for the six designed modes: (a–c) single-beam results; (d–f) dual-beam results, including the comparison between the measurement results and the simulation results.

### 6. Conclusions

In this paper, a dual-polarized 2-bit intelligent reflection surface based on a paper-based flexible substrate is proposed. Compared to traditional reconfigurable metasurfaces that depend on active structures and are manufactured using PCB technology, this innovative IRS design boasts several outstanding features in the context of large-scale communications. It eliminates the need for complex active structures, significantly reducing production costs and energy consumption while offering enhanced flexibility and integrability. Its practicality and low-cost production make it a promising option for large-scale 6G network deployment. By manufacturing rotationally symmetric small metal block structures on paper using silver ink, four structures are obtained that achieve a phase difference of

90 degrees for both x-polarized and y-polarized wave incidence at the resonant frequency of 4.5754 GHz, enabling customized scattering effects via the arrangement of the units. The measurements agree well with our design and simulations, achieving a high degree of overlap in the range of  $-30^\circ$  to  $+30^\circ$ , and the amplitude measurements are within  $\pm 0.3$  dB of the simulation results, implying a high degree of accuracy in our design. The IRS structure allows for precise control of electromagnetic waves and provides more degrees of freedom for beam control, thereby improving the performance and functionality of communication systems. Moreover, the paper-based metasurface is low-cost, highly portable, and suitable for IRS wireless communication applications, radar systems, and remote sensing applications. In real communication scenarios, fast reconfigurable switching is not the most urgent requirement, but power consumption and low cost are. Therefore, this work is expected to have important application value in related fields of wireless communications. Potential future directions for the technology include the integration of dual-polarized infrared spectroscopy with advanced communication systems, and further research in these areas is expected to open up new possibilities for its practical application.

**Author Contributions:** Conceptualization, X.J.; methodology, H.T.; software, X.D.; validation, H.T. and F.Y.; formal analysis, H.T.; investigation, H.C.; writing—original draft preparation, H.T.; writing—review and editing, F.Y.; visualization, X.D.; project administration, H.C.; funding acquisition, L.C. All authors have read and agreed to the published version of the manuscript.

**Funding:** This work was funded by the National Key Research and Development Program of the National Natural Science Foundation of China, grant numbers 11404207 and 52177185; SHIEP Foundation, grant numbers K2014-054 and Z2015-086; and the Local Colleges and Universities Capacity Building Program of the Shanghai Science and Technology Committee, China, grant number 15110500900.

**Institutional Review Board Statement:** Not applicable.

**Informed Consent Statement:** Not applicable.

**Data Availability Statement:** The data presented in this study are available on request from the corresponding author.

**Conflicts of Interest:** The authors declare no conflicts of interest.

## References

1. Dang, S.; Amin, O.; Shihada, B.; Alouini, M.-S. What should 6G be? *Nat. Electron.* **2020**, *3*, 20–29. [[CrossRef](#)]
2. Chowdhury, M.Z.; Shahjalal, M.; Ahmed, S.; Jang, Y.M. 6G wireless communication systems: Applications, requirements, technologies, challenges, and research directions. *IEEE Open J. Commun. Soc.* **2020**, *1*, 957–975. [[CrossRef](#)]
3. Gu, Z.; Ma, Q.; Gao, X.; You, J.W.; Cui, T.J. Classification of Metal Handwritten Digits Based on Microwave Diffractive Deep Neural Network. *Adv. Opt. Mater.* **2023**, 2301938. [[CrossRef](#)]
4. Ma, Q.; Shi, C.B.; Chen, T.Y.; Qi, M.Q.; Li, Y.B.; Cui, T.J. Broadband metamaterial lens antennas with special properties by controlling both refractive-index distribution and feed directivity. *J. Opt.* **2018**, *20*, 045101. [[CrossRef](#)]
5. Gao, X.; Ma, Q.; Gu, Z.; Cui, W.Y.; Liu, C.; Zhang, J.; Cui, T.J. Programmable surface plasmonic neural networks for microwave detection and processing. *Nat. Electron.* **2023**, *6*, 319–328. [[CrossRef](#)]
6. You, J.W.; Ma, Q.; Lan, Z.; Xiao, Q.; Panoiu, N.C.; Cui, T.J. Reprogrammable plasmonic topological insulators with ultrafast control. *Nat. Commun.* **2021**, *12*, 5468. [[CrossRef](#)] [[PubMed](#)]
7. Li, Y.; Chen, S.; Liang, H.; Ren, X.; Luo, L.; Ling, Y.; Liu, S.; Su, Y.; Wu, S.-T. Ultracompact multifunctional metalens visor for augmented reality displays. *Photonix* **2022**, *3*, 29. [[CrossRef](#)]
8. Ma, Q.; Hong, Q.R.; Gao, X.X.; Jing, H.B.; Liu, C.; Bai, G.D.; Cheng, Q.; Cui, T.J. Smart sensing metasurface with self-defined functions in dual polarizations. *Nanophotonics* **2020**, *9*, 3271–3278. [[CrossRef](#)]
9. Ma, Q.; Bai, G.D.; Jing, H.B.; Yang, C.; Li, L.; Cui, T.J. Smart metasurface with self-adaptively reprogrammable functions. *Light Sci. Appl.* **2019**, *8*, 98. [[CrossRef](#)]
10. Liu, C.; Ma, Q.; Luo, Z.J.; Hong, Q.R.; Xiao, Q.; Zhang, H.C.; Miao, L.; Yu, W.M.; Cheng, Q.; Li, L. A programmable diffractive deep neural network based on a digital-coding metasurface array. *Nat. Electron.* **2022**, *5*, 113–122. [[CrossRef](#)]
11. Wang, H.; Zhan, Z.; Hu, F.; Meng, Y.; Liu, Z.; Fu, X.; Liu, Q. Intelligent optoelectronic processor for orbital angular momentum spectrum measurement. *Photonix* **2023**, *4*, 9. [[CrossRef](#)]
12. Liu, C.; Yu, W.M.; Ma, Q.; Li, L.; Cui, T.J. Intelligent coding metasurface holograms by physics-assisted unsupervised generative adversarial network. *Photonics Res.* **2021**, *9*, B159–B167. [[CrossRef](#)]

13. Tan, Z.; Yi, J.; Cheng, Q.; Burokur, S.N. Design of perfect absorber based on metagratings: Theory and experiment. *IEEE Trans. Antennas Propag.* **2023**, *71*, 1832–1842. [[CrossRef](#)]
14. Chen, L.; Ma, Q.; Luo, S.S.; Ye, F.J.; Cui, H.Y.; Cui, T.J. Touch-Programmable Metasurface for Various Electromagnetic Manipulations and Encryptions. *Small* **2022**, *18*, e2203871. [[CrossRef](#)] [[PubMed](#)]
15. Chen, L.; Ma, Q.; Nie, Q.F.; Hong, Q.R.; Cui, H.Y.; Ruan, Y.; Cui, T.J. Dual-polarization programmable metasurface modulator for near-field information encoding and transmission. *Photonics Res.* **2021**, *9*, 116–124. [[CrossRef](#)]
16. Gu, Z.; Ma, Q.; Liu, C.; Xiao, Q.; Gao, X.; Yan, T.; Miao, L.; Li, L.; Cui, T.J. High-Resolution Programmable Metasurface Imager Based on Multilayer Perceptron Network. *Adv. Opt. Mater.* **2022**, *10*, 2200619. [[CrossRef](#)]
17. Tang, W.; Chen, M.Z.; Dai, J.Y.; Zeng, Y.; Zhao, X.; Jin, S.; Cheng, Q.; Cui, T.J. Wireless communications with programmable metasurface: New paradigms, opportunities, and challenges on transceiver design. *IEEE Wirel. Commun.* **2020**, *27*, 180–187. [[CrossRef](#)]
18. Zhao, J.; Yang, X.; Dai, J.Y.; Cheng, Q.; Li, X.; Qi, N.H.; Ke, J.C.; Bai, G.D.; Liu, S.; Jin, S. Programmable time-domain digital-coding metasurface for non-linear harmonic manipulation and new wireless communication systems. *Natl. Sci. Rev.* **2019**, *6*, 231–238. [[CrossRef](#)]
19. Ma, Q.; Gao, W.; Xiao, Q.; Ding, L.; Gao, T.; Zhou, Y.; Gao, X.; Yan, T.; Liu, C.; Gu, Z.; et al. Directly wireless communication of human minds via non-invasive brain-computer-metasurface platform. *eLight* **2022**, *2*, 11. [[CrossRef](#)]
20. Cui, T.J.; Qi, M.Q.; Wan, X.; Zhao, J.; Cheng, Q. Coding metamaterials, digital metamaterials and programmable metamaterials. *Light Sci. Appl.* **2014**, *3*, e218. [[CrossRef](#)]
21. Cui, T.J.; Li, L.; Liu, S.; Ma, Q.; Zhang, L.; Wan, X.; Jiang, W.X.; Cheng, Q. Information Metamaterial Systems. *iScience* **2020**, *23*, 101403. [[CrossRef](#)] [[PubMed](#)]
22. Ma, Q.; Liu, C.; Xiao, Q.; Gu, Z.; Gao, X.X.; Li, L.; Cui, T.J. Information metasurfaces and intelligent metasurfaces. *Photonics Insights* **2022**, *1*, R01. [[CrossRef](#)]
23. Ma, Q.; Xiao, Q.; Hong, Q.R.; Gao, X.; Galdi, V.; Cui, T.J. Digital Coding Metasurfaces: From Theory to Applications. *IEEE Antennas Propag. Mag.* **2022**, *64*, 96–109. [[CrossRef](#)]
24. He, Q.; Sun, S.; Zhou, L. Tunable/reconfigurable metasurfaces: Physics and applications. *Research* **2019**, *2019*, 1849272. [[CrossRef](#)] [[PubMed](#)]
25. Dai, L.; Wang, B.; Wang, M.; Yang, X.; Tan, J.; Bi, S.; Xu, S.; Yang, F.; Chen, Z.; Di Renzo, M. Reconfigurable intelligent surface-based wireless communications: Antenna design, prototyping, and experimental results. *IEEE Access* **2020**, *8*, 45913–45923. [[CrossRef](#)]
26. Chen, L.; Ma, H.L.; Cui, H.Y. Wavefront manipulation based on mechanically reconfigurable coding metasurface. *J. Appl. Phys.* **2018**, *124*, 043101. [[CrossRef](#)]
27. Gros, J.-B.; Popov, V.; Odit, M.A.; Lenets, V.; Lerosey, G. A reconfigurable intelligent surface at mmWave based on a binary phase tunable metasurface. *IEEE Open J. Commun. Soc.* **2021**, *2*, 1055–1064. [[CrossRef](#)]
28. Darvazehban, A.; Rezaeieh, S.A.; Zamani, A.; Abbosh, A.M. Pattern reconfigurable metasurface antenna for electromagnetic torso imaging. *IEEE Trans. Antennas Propag.* **2019**, *67*, 5453–5462. [[CrossRef](#)]
29. Ptilakis, A.; Tsilipakos, O.; Liu, F.; Kossifos, K.M.; Tasolamprou, A.C.; Kwon, D.-H.; Mirmoosa, M.S.; Manassis, D.; Kantartzis, N.V.; Liaskos, C. A multi-functional reconfigurable metasurface: Electromagnetic design accounting for fabrication aspects. *IEEE Trans. Antennas Propag.* **2020**, *69*, 1440–1454. [[CrossRef](#)]
30. Del Hougne, P.; Imani, M.F.; Diebold, A.V.; Horstmeyer, R.; Smith, D.R. Learned integrated sensing pipeline: Reconfigurable metasurface transceivers as trainable physical layer in an artificial neural network. *Adv. Sci.* **2020**, *7*, 1901913. [[CrossRef](#)]
31. Jiang, R.Z.; Ma, Q.; Gu, Z.; Liang, J.C.; Xiao, Q.; Cheng, Q.; Cui, T.J. Simultaneously Intelligent Sensing and Beamforming Based on an Adaptive Information Metasurface. *Adv. Sci.* **2023**, e2306181. [[CrossRef](#)] [[PubMed](#)]
32. Wan, X.; Qi, M.Q.; Chen, T.Y.; Cui, T.J. Field-programmable beam reconfiguring based on digitally-controlled coding metasurface. *Sci. Rep.* **2016**, *6*, 20663. [[CrossRef](#)] [[PubMed](#)]

**Disclaimer/Publisher’s Note:** The statements, opinions and data contained in all publications are solely those of the individual author(s) and contributor(s) and not of MDPI and/or the editor(s). MDPI and/or the editor(s) disclaim responsibility for any injury to people or property resulting from any ideas, methods, instructions or products referred to in the content.